Report of Numerical results of Problem A Using RFPA^{3D}-CT

Huihui Zhang(1), Xiaotian Wu(2), Tianjiao Li(3)

School of Civil Engineering (Dalian University of Technology)

Dalian, China

huihzhang@126.com

Abstract—**RFPA^{3D}-CT was used to solve Problem A about rock fracturing. RFPA is based on the idea that heterogeneity leads to macro nonlinearity and causes progressive failure behavior observed in brittle rock. The modeling was divided into two stages. The first stage was to determine the numerical parameters. The second stage was to predict the results under given conditions. In this report, the uniaxial compressive strength and the failure pattern of the specimens were given based on simulation. In stage 1, the relative error of uniaxial compressive strength between numerical results and experimental results were less than 6%. In stage 2, it was found that Model (d) has the greatest elastic modulus and Model (b) has the lowest strength. The fracture path was determined by both initial fractures, loadings and end effects.**

Keywords—RFPA^{3D}, Uniaxial Compressive Strength, fracture, meso-element

I. Numerical methods and software

In this paper, FEM based 3D simulator RFPA-CT is used to simulate uniaxial compression tests. It is based on the idea that the heterogeneity leads to macro nonlinearity and causes progressive failure behavior observed in brittle rock[1, 2].Therefore, global non-linear behaviors observed in brittle rock can be simulated with brittle-elastic elements differing in strength and elastic constant parameters depending on the heterogeneity index of the rock materials[1]. When the pre-described strength is reached, the assumed parameters of the failed elements vary to describing its weak and soft mechanical properties[1]. During the progressive failure process, failed elements connect to form a fracture, and no sliding interface or special "gap" element is needed[1]. RFPA has its own excellent characteristics. It does not require remeshing after each time step or adding any artificial boundary element when the fracture propagates. It results in lower computation time and is well-suited for modeling fractures[3, 4].

RFPA-CT with FEM capability was implemented as a basic simulator for geomechanical analysis. In RFPA-CT, the eight-node isoparametric hexahedral element

is used as the basic element[5]. It is developed with the following assumptions: A fractured porous rock is assumed to be an inhomogenous, isothermal, deformable fluid-saturated porous medium. Its heterogeneity is considered by assuming that the properties, such as Young's modulus and the strength properties of each element, conform to the Weibull distribution (specified by the Weibull distribution parameters)[2, 5]. At the elemental scale, the rock mass is treated as an elastobrittle material with a residual strength[5, 6]. Its mechanical behavior is modeled by an elastic damage constitutive law, and the residual strain/deformation upon unloading is not considered[5, 6]. Additionally, the coupled process between stress/strain and fluid flow in the deforming rock mass is governed by Biot's consolidation theory[7].

In RFPA-CT, the stress and strain are negative in compression and positive in tension. In the geomechanical model, elastic mechanics for an isotropic linear poroelastic medium is used to describe rock deformation at the elemental scale before damage [3, 4, 8], including the following constitutive relations:

$$\boldsymbol{\sigma}=2G\boldsymbol{\varepsilon}+\frac{2\upsilon G}{1-2\upsilon}tr(\boldsymbol{\varepsilon})\mathbf{I}-\alpha P\mathbf{I}-K\alpha_v\Delta T\mathbf{I} \tag{1}$$

$$P=\sum_\beta S_\beta P_\beta \tag{2}$$

While the equations of equilibrium and the strain–displacement relation can be expressed as:

$$\nabla\cdot\boldsymbol{\sigma}+\mathbf{f}=0 \tag{3}$$

and

$$\boldsymbol{\varepsilon}=\frac{1}{2}((\nabla\mathbf{u})^T+\nabla\mathbf{u}) \tag{4}$$

Mechanical properties and permeability characteristics of rock are different. They lead to great spatial heterogeneity in mesoscopic properties of rock[5]. In RFPA-CT modeling, the material is composed of many elements whose material parameters (such as Young's modulus and strength) is assumed to follow a Weibull function with threshold values[5, 9], as:

$$f(x)=\frac{m}{x_0}\left(\frac{x}{x_0}\right)^{m-1}\exp\left(-\frac{x}{x_0}\right)^m \tag{5}$$

According to this function, main input material parameters can be determined.

An element assumed to be elastobrittle with a residual strength has only one failure mode. Its load-displacement relationship is shown in Fig.1. It is considered to fail in a tensile mode when the minimum principal stain exceeds the experimentally determined uniaxial tensile strain at failure or the minimum principal stress exceeds the uniaxial tensile strength[10]and fail in a shear mode when the shear stress satisfies the Mohr-

Coulomb failure criterion[3, 4]. The failure criterions (including the maximum strain criterion, the maximum stress criterion and the Mohr-Coulomb failure criterion) are expressed as flowing in equations:

$$\varepsilon_3 \leq -\frac{\sigma_{t0}}{E} \tag{6}$$

or

$$\sigma_3 \leq -\sigma_{t0} \tag{7}$$

or

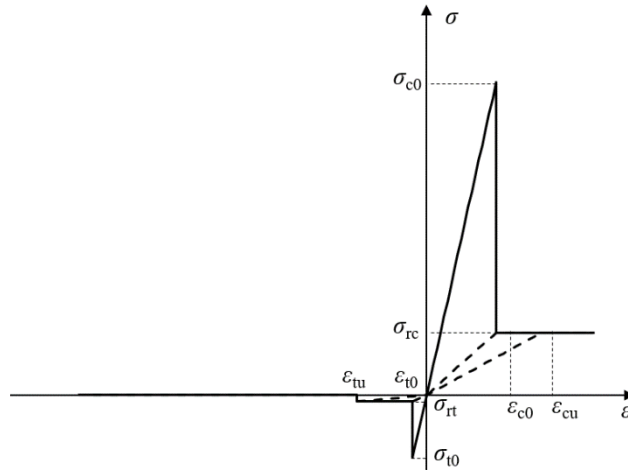$$\sigma_1 - \sigma_3 \frac{1+\sin\phi}{1-\sin\phi} \geq \sigma_{c0} \tag{8}$$

Figure 1 Elastic damage constitutive law of an element under uniaxial stress

When element's state satisfies any one of these criterions, the element begins to accumulate damage[3, 4]. In elastic damage mechanics, the elastic modulus of the element gradually decreases with damage[3, 4]. Based on the assumption of equivalent strain principle, the elastic modulus of the damaged element is given by:

$$E_d = (1-D)E_0 \tag{9}$$

The damage variable of an element in a tensile mode under multiaxial stress states can be expressed as[5, 11-13]:

$$D = \begin{cases} 0 & \bar{\varepsilon} > \varepsilon_{t0} \\ 1 - \dfrac{\sigma_{rt}}{\bar{\varepsilon}E_0} & \varepsilon_{tu} < \bar{\varepsilon} \leq \varepsilon_{t0} \\ 1 & \bar{\varepsilon} \leq \varepsilon_{tu} \end{cases} \tag{10}$$

$$\varepsilon_{tu} = \eta \varepsilon_{t0} \tag{11}$$

where $\bar{\varepsilon}$ is the equivalent principal strain. It is defined as follows[11, 14]:

$$\varepsilon = -\sqrt{\left\langle -\varepsilon_1^2 \right\rangle + \left\langle -\varepsilon_2^2 \right\rangle + \left\langle -\varepsilon_3^2 \right\rangle} \tag{12}$$

where ε_1, ε_2 and ε_3 are the three principal strains, and $\langle \ \rangle$ is a function defined as follows:

$$\langle x \rangle = \begin{cases} x & x \geq 0 \\ 0 & x < 0 \end{cases} \tag{13}$$

The damage variable of an element in a shear mode under multiaxial stress states can be expressed as[5, 11-13]:

$$D = \begin{cases} 0 & \varepsilon_1 < \varepsilon_{c0} \\ 1 - \dfrac{\sigma_{rc}}{\varepsilon_1 E_0} & \varepsilon_{c0} \leq \varepsilon_1 \end{cases} \tag{14}$$
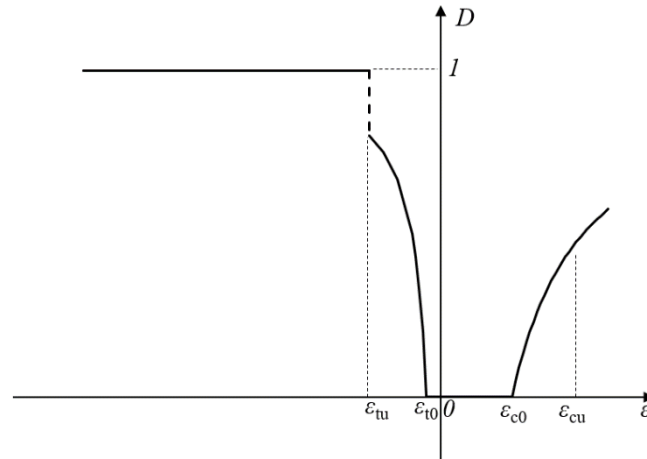

Figure 2 Damage variable of an element (the x-axis is equivalent principal strain for tensile failure mode and maximum principal strain for shear failure mode)
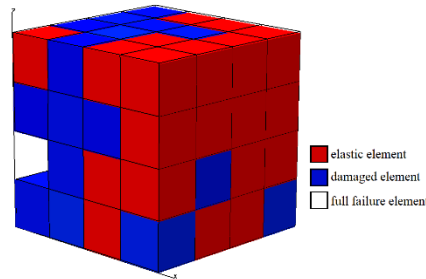

Figure 3 Schematics showing the elastic elements, damaged elements and failure

elements in RFPA[3, 4]

In RFPA-CT, the state of elements can be classified by damage variable into three kinds that are elastic element (D=0), damaged element ($0<D<1$) and full failure element (D=1). They are distinguished by different colors as shown in Figure 3[3, 4].

II. Numerical modelling

Specimens (Granite, Marble, and Red-sandstone) with 50 mm in height and length, 30 mm in width were under constant strain rate conditions (1 mm/min) to get the uniaxial compressive strength (UCS).

The dimension of the uniaxial compressive numerical model was the same as the experimental specimens. It was meshed by elements with a side length of 0.5 mm or 1 mm. The numerical model was loaded from the top by a constant displacement rate of 0.005mm/step. Two strong plates were set on the top and the bottom of the model to consider the end effect. The configuration and boundary conditions of the numerical model are shown in Figure 4.
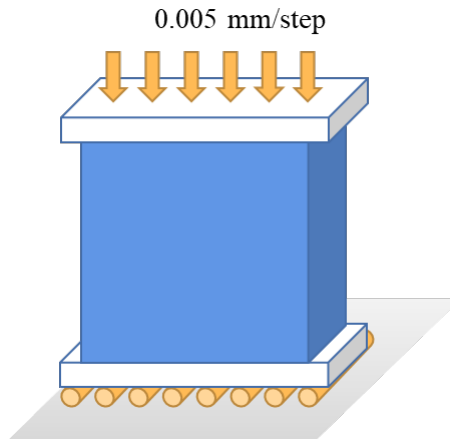

Figure 4 Configuration of the numerical model

III. Clabration results

(i) Parameter determination of validation model 1

The numerical parameters are adjusted based on comparing the simulated load-displacement curve with the laboratory one. The mean mesoscopic Young's modulus E_0 and strength σ_{c0} and other mechanical parameters, which are used in the stage 2 were estimated through modeling of uniaxial compression. First, the approximate mesoscopic values are gained from the following regression equations:

$$\frac{\sigma_c}{\sigma_{c0}} = 0.2602 \ln m + 0.0233 \quad (1.2 \le m \le 50) \qquad (34)$$

$$\frac{E}{E_0} = 0.1412 \ln m + 0.6476 \quad (1.2 \le m \le 10) \qquad (35)$$

Then, those values are adjusted based on comparing the simulated load-displacement curve with the laboratory one. After simulation tests, the mesoscopic mechanical parameters are shown in Table 1.

Table 1 The mechanical and physical parameters used in RFPA simulation

Parameter	Symbol	Unit	Granite	Marble	Red-sandstone
Geometry		mm*mm*mm		50×30×50	
Mesh		-		100*30*100	
Homogeneity index	m	-	3	3	1.5
Mean mesoscopic Young's modulus	E_0	GPa	18.5	40	21
Mean mesoscopic strength	σ_{c0}	MPa	700	580	780
Poisson's ratio	v	-	0.265	0.274	0.225
Friction angle	φ	°	50	50	50
Compression-tension ratio	-	-	20	20	20
Residual strength coefficient	λ	-	0.1	0.1	0.1
Ultimate tensile strain coefficient	η_t	-	5	5	5
Ultimate compressive strain coefficient	η_c	-	200	200	200

(ii) Modeling Results of validation model 1

The simulated uniaxial compressive strength (UCS) of three types of intact rocks were listed in Table2 The load-displacement curves and failure types of representative specimens are shown in Figure 5 and Figure 6, respectively.

Table 2 Modelling results of three types of intact rocks in uniaxial compression tests

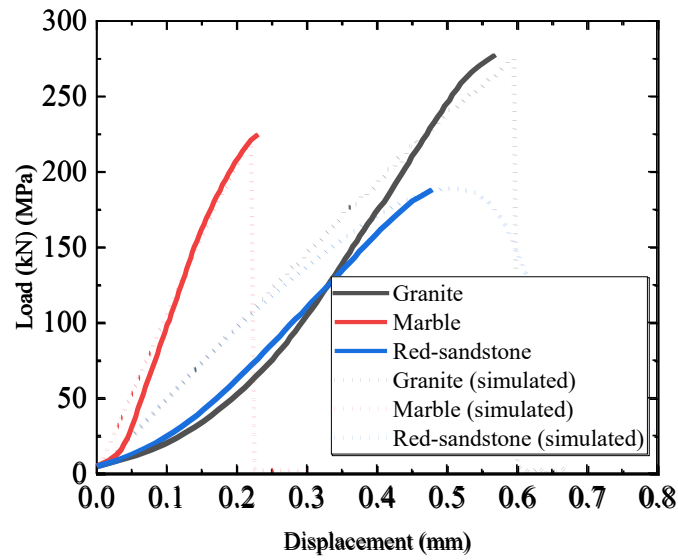| Parameters	UCS (MPa)	Relative error
Granite	183.33	0.3%
Marble	148.00	1.3%
Red-sandstone	126.00	0.8%

Figure 5 Load-Displacement curves of the numerical uniaxial compression model and data for intact rock specimens of validation model 1.
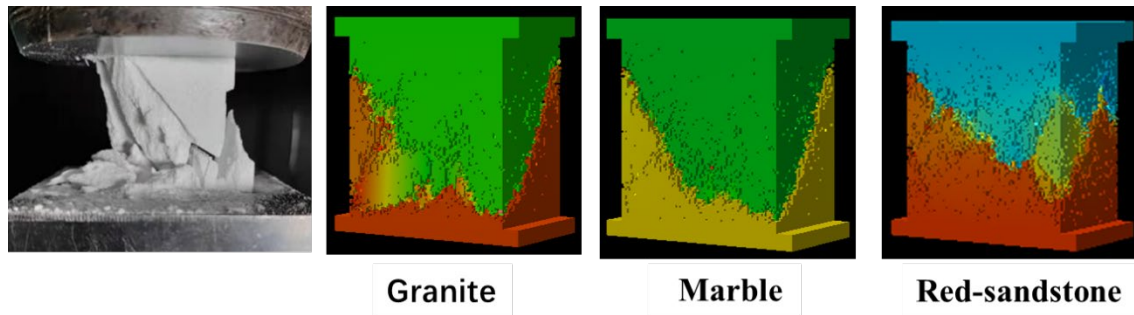

Figure 6 Failure shapes of the numerical uniaxial compression model and the intact rock specimens of validation model 1.

(iii) Parameter determination of validation model 2

After simulation tests, the mesoscopic mechanical parameters are shown in Table 3.

Table 3 The mechanical and physical parameters used in RFPA simulation

Parameter	Symbol	Unit	Granite	Marble	Red-sandstone
Geometry		$mm*mm*mm$		$50\times30\times50$	
Mesh		-		$100*30*100$	
Homogeneity index	m	-	3	3	1.5
Mean mesoscopic Young's modulus	E_0	GPa	23	50	25
Mean mesoscopic strength	σ_{c0}	MPa	700	580	700
Poisson's ratio	v	-	0.265	0.274	0.225
Friction angle	φ	°	50	50	50
Compression-tension ratio	-	-	20	20	20
Residual strength coefficient	λ	-	0.1	0.1	0.1
Ultimate tensile strain coefficient	η_t	-	5	5	5
Ultimate compressive strain coefficient	η_c	-	200	200	200

(iv) Modeling Results of validation model 2

The simulated uniaxial compressive strength (UCS) of three types of rocks with initial fractures (validation model 2) were listed in Table 4. The load-displacement curves and failure types of representative specimens are shown in Figure 7 and Figure 8, respectively.

Table 4 Modelling results of three types of rocks in uniaxial compression tests of validation model 2

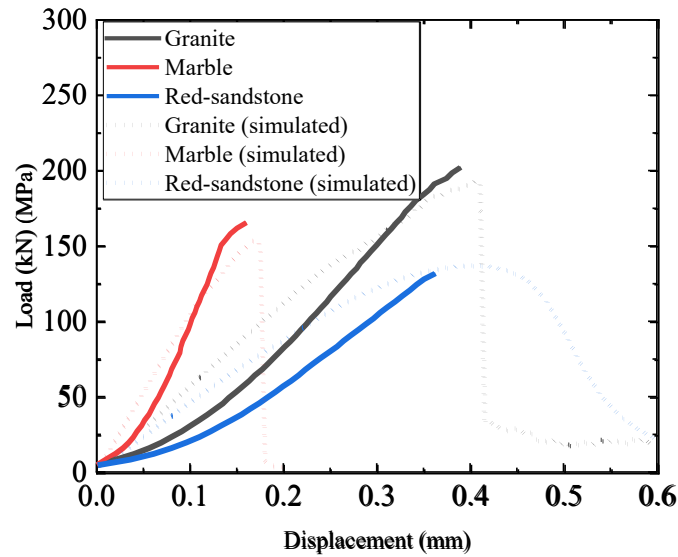| Parameters	UCS (MPa)	Relative error
Granite	128.67	4%
Marble	103.33	6%
Red-sandstone	91.33	3%

Figure 7 Load-Displacement curves of the numerical uniaxial compression model and data for specimens of validation model 2.
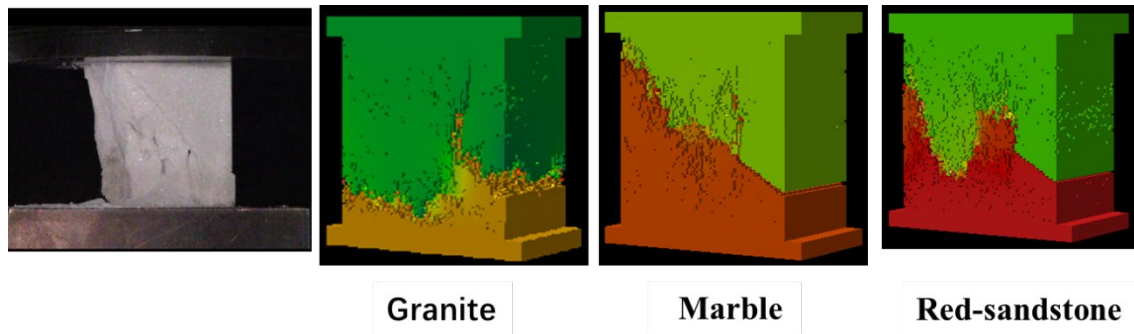

Figure 8 Failure shapes of the numerical uniaxial compression model and the specimens of validation model 2.

IV. Prediction results

The four types of preset crack for marble samples subjected to uniaxial compression test are given in Figure 9. The simulated uniaxial compressive strength (UCS) of three types of rocks with initial fractures were listed in Table 5. The predicted load-displacement curves and failure types of specimens are shown in Figure 10 and Figure 11, respectively. From Table 5 and Figure 10, it is found that Model D has the greatest elastic modulus, and Model B has the lowest strength. Figure 11 shows the predicted fractured paths were almost along with the initial fractures.
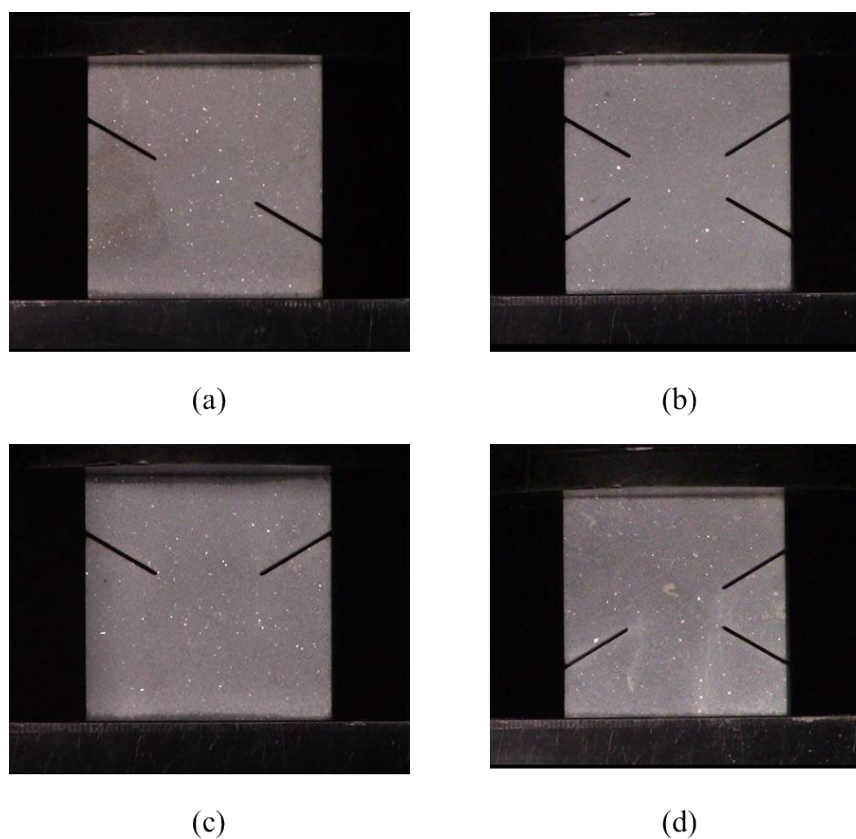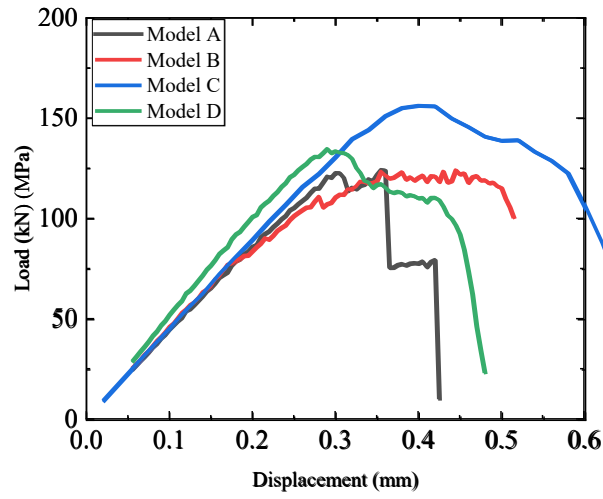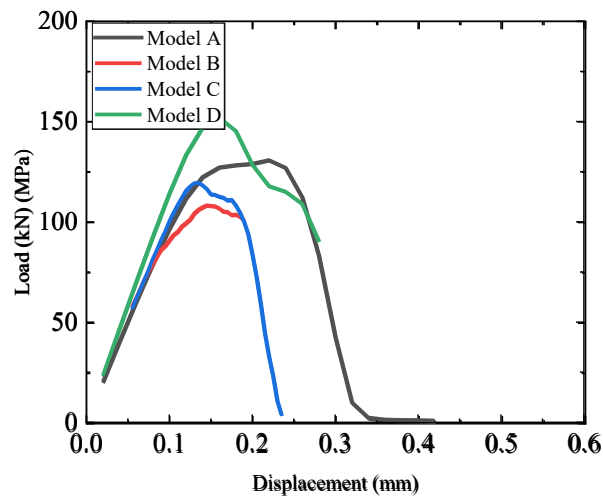
(a)

(b)

(c)

(d)

Figure 9   Four types of preset crack samples subjected to uniaxial compression test

Table 5 Modelling results of three types of rocks in uniaxial compression tests of validation model 2
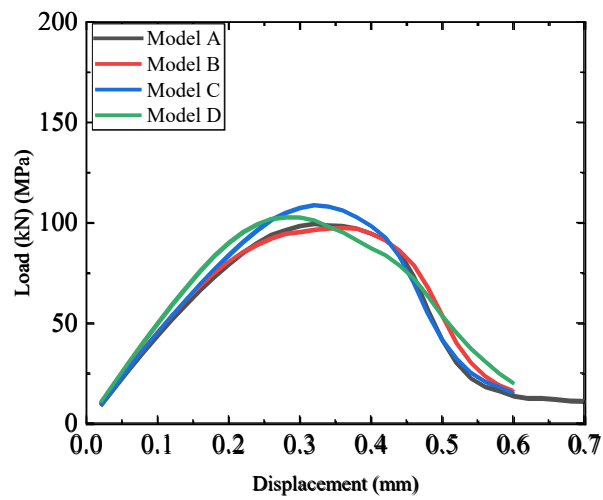
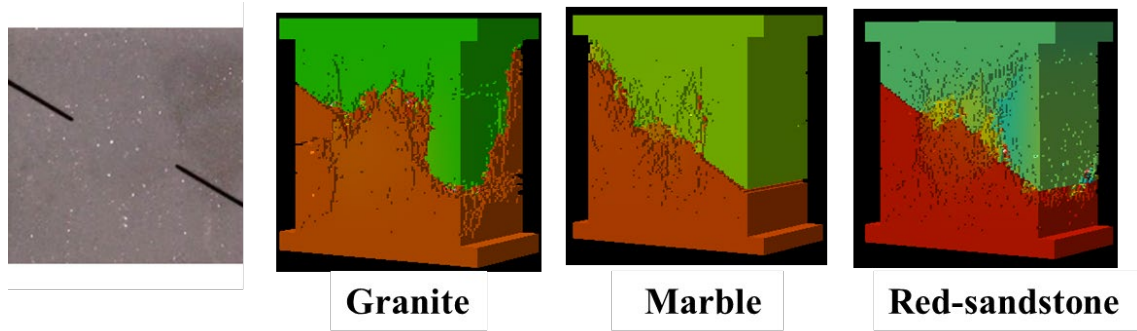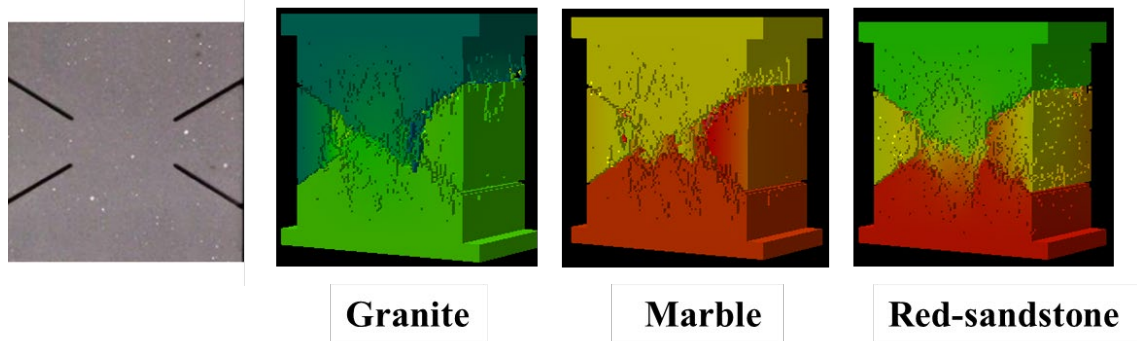| Parameters	UCS (MPa)			
	(a)	(b)	(c)	(d)
Granite	81.80	82.07	103.73	89.80
Marble	87.13	72.00	79.73	101.33
Red-sandstone	66.33	65.00	72.53	68.53

(a) Granite

(b) Marble
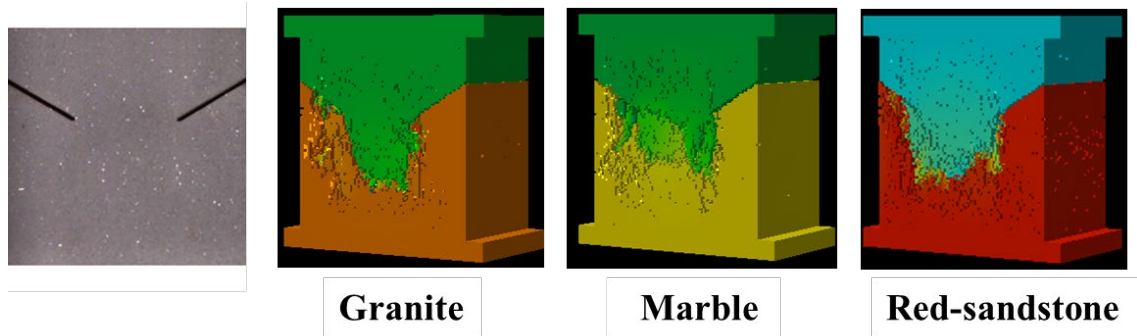

(c) Red-sandstone

Figure 10 The predicted load-Displacement curves of the numerical uniaxial compression model.
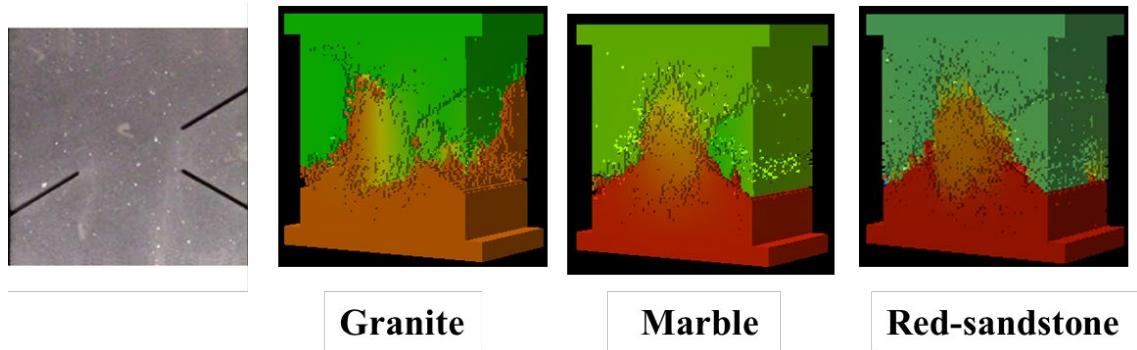
(a) Model a

(b) Model b

(c) Model c

(d) Model d

Figure 11 The predicted failure shapes of the numerical uniaxial compression model.

V. Conclusions

RFPA^{3D}-CT was used to solve Problem A about rock fracturing. RFPA is based on the idea that heterogeneity leads to macro nonlinearity and causes progressive failure behavior observed in brittle rock. In this report, the uniaxial compressive strength and the failure pattern of the specimens were given based on simulation. In stage 1, the relative error of uniaxial compressive strength between numerical results and experimental results were less than 6%. In stage 2, it was found that Model (d) has the greatest elastic modulus, and Model (b) has the lowest strength. The predicted fractured paths were almost along with the initial fractures. The fracture path was determined by both initial fractures, loadings and end effects. The Granite has higher strength no matter the intact rock or the rock with initial fractures in general.

VI. Acknowledgment

References:

1. Tang C, Tang C. Numerical simulation of progressive rock failure and associated seismicity. International Journal of Rock Mechanics & Mining Sciences. 1997;34:249-61.

2. Tang CA, Yang WT, Fu YF, Xu XH. A new approach to numerical method of modelling geological processes and rock engineering problems—continuum to discontinuum and linearity to nonlinearity. ENG GEOL. 1998;49:207-14.

3. Li T, Li L, Tang C, Zhang Z, Li M, Zhang L, et al. A coupled hydraulic-mechanical-damage geotechnical model for simulation of fracture propagation in geological media during hydraulic fracturing. J PETROL SCI ENG. 2019;173:1390-416.

4. Li T, Tang C, Rutqvist J, Hu M. TOUGH-RFPA: Coupled thermal-hydraulic-mechanical rock failure process analysis with application to deep geothermal wells. INT J ROCK MECH MIN. 2021;142:104726.

5. Li LC, Tang CA, Wang SY, Yu J. A Coupled Thermo-Hydrologic-Mechanical Damage Model and Associated Application in a Stability Analysis On a Rock Pillar. TUNN UNDERGR SP TECH. 2013;34:38-53.

6. Li LC, Li G, Wang SY, Liang ZZ, Zhang YB. Numerical Simulation of 3D Hydraulic Fracturing Based on an Improved Flow-Stress-Damage Model and a Parallel FEM Technique. Rock Mechanics & Rock Engineering. 2012;45:801-18.

7. Biot MA. General theory of three‐dimensional consolidation. J APPL PHYS. 1941;12:155-64.

8. Zhou L, Hou MZ. A new numerical 3D-model for simulation of hydraulic fracturing in consideration of hydro-mechanical coupling effects. INT J ROCK MECH MIN. 2013;60:370-80.

9. Li G, Tang C, Li L, Li H. An Unconditionally Stable Explicit and Precise Multiple Timescale Finite Element Modeling Scheme for the Fully Coupled Hydro-Mechanical Analysis of Saturated Poroelastic Media. COMPUT GEOTECH. 2016;71:69-81.

10. Rankine WJM. Manual of applied mechanics. C.griffen Co. 2013.

11. Li Z, Li L, Huang B, Zhang L, Li M, Zuo J, et al. Numerical investigation on the propagation

behavior of hydraulic fractures in shale reservoir based on the DIP technique. J PETROL SCI ENG. 2017;154:302-14.

12. Li Z, Li L, Li M, Zhang L, Zhang Z, Huang B, et al. A numerical investigation on the effects of rock brittleness on the hydraulic fractures in the shale reservoir. J NAT GAS SCI ENG. 2018;50:22-32.

13. Liang ZZ, Tang CA, Li HX, Zhang YB. Numerical simulation of the 3-D failure process in heterogeneous rocks. International Journal of Rock Mechanics & Mining Sciences. 2004;41:419.

14. Ruoqiong ZWYG. Elasto brittle damage model for rockmass based on field tests in Laxiwa arch dam site [J]. Chinese Jounal of Geotechnical Engineering. 1998;5.